Optics Letters

Single-photon stored-light Ramsey interferometry using Rydberg polaritons

Yuechun Jiao,[1,2] Nicholas L. R. Spong,[1] Oliver D. W. Hughes,[1] Chloe So,[1] Teodora Ilieva,[1] Kevin J. Weatherill,[1] and Charles S. Adams[1,*]

[1]Joint Quantum Centre (Durham-Newcastle), Department of Physics, Durham University, South Road, Durham DH1 3LE, UK
[2]State Key Laboratory of Quantum Optics and Quantum Optics Devices, Institute of Laser Spectroscopy, Shanxi University, Taiyuan 030006, China
*Corresponding author: c.s.adams@durham.ac.uk

Received 12 August 2020; revised 17 September 2020; accepted 18 September 2020; posted 21 September 2020 (Doc. ID 405143); published 15 October 2020

We demonstrate a single-photon stored-light interferometer, where a photon is stored in a laser-cooled atomic ensemble in the form of a Rydberg polariton with a spatial extent of $10 \times 1 \times 1\ \mu m^3$. The photon is subject to a Ramsey sequence, i.e., "split" into a superposition of two paths. After a delay of up to 450 ns, the two paths are recombined to give an output dependent on their relative phase. The superposition time of 450 ns is equivalent to a free-space propagation distance of 135 m. We show that the interferometer fringes are sensitive to external fields and suggest that stored-light interferometry could be useful for localized sensing applications.

https://doi.org/10.1364/OL.405143

Interferometers [1] are versatile tools in engineering, oceanography, seismology, metrology, and astronomy [2]. Replacing photons by massive particles creates an interferometer [3] that is sensitive to gravity and other inertial effects. Interferometry using the internal quantum states of atoms [4,5] has become an important technique in the measurement of time and quantum coherence. Hybrid light–matter interferometers are also possible. In a slow-light interferometer [6], the field is partly photonic and partly atomic. A hybrid atom–light interferometer using internal atomic states to form a beam splitter has also been demonstrated [7,8]. Interferometry using atomic Rydberg states is useful in the detection of electric fields, as demonstrated using individual atoms [9], atomic beams [10], and Rydberg-dressed cold-atom ensembles [11]. For all types of interferometry, the measurement sensitivity is limited by the time between the splitting and recombination processes, which is typically proportional to the length of the interferometer arms.

Here, we propose and demonstrate a hybrid interferometer based on a single photon stored as a spin wave in a cold atomic gas. The advantage of using stored light (or slow light) is that superposition time is decoupled from the size of the interferometer. For example, we demonstrate a quantum superposition time of 450 ns—equivalent to a free-space interferometer path length of 135 m—using an interferometer localized to a few micrometers. The two paths of the interferometer are formed by driving the spin wave into a superposition of quantum states. We employ highly excited Rydberg states, which allows the splitting and recombining of the optical paths to be performed using a microwave field. Similar to other Rydberg experiments [9–11], the output is sensitive to DC and AC electric fields. As the interferometer is localized over a length scale of only a few micrometers, the Rydberg blockade mechanism [12] forces the interferometer to operate with only one photon at a time. This has the advantage that phase shifts due to atom–atom interactions are suppressed. Both localization and the single-photon character may be advantageous in some measurement applications, such as sensing and imaging [9,13–15].

The principle of our single-photon stored-light interferometer is illustrated in Fig. 1. To store a photon, first laser-cooled ^{87}Rb atoms are loaded into an 862 nm optical dipole trap with a waist of $w_r = 4.5\ \mu m$ and a trap depth of ~ 0.5 mK. The atoms are optically pumped into the $|g\rangle = |5S_{1/2}, F = 2, m_F = 2\rangle$ sublevel. Next, we illuminate the laser-cooled atomic ensemble with both a probe laser (780 nm) and a control laser (480 nm) for 500 ns. The probe beam, resonant with the $|g\rangle = |5S_{1/2}, F = 2, m_F = 2\rangle \rightarrow |e\rangle = |P_{3/2}, F' = 3, m'_F = 3\rangle$ transition, is focused into the ensemble with a beam waist of 1.5 μm. The control beam, resonant with the $|e\rangle \rightarrow |r\rangle = |nS_{1/2}\rangle$ transition, is focused to a waist of 25 μm. The probe and control beams are circularly polarized and counter-propagate. The incoming probe pulses have mean photon numbers less than two, $n_s^{\text{in}} = 1.3$, and the Rabi frequency of the control beam is $\Omega_c = 2\pi \times 13.2$ MHz at 60S. Before the probe is switched off, the control beam is ramped down to zero, storing a signal photon as a collective Rydberg excitation [16]. The spatial extent of the stored photon is of order $10 \times 1 \times 1\ \mu m^3$. The storage and retrieval efficiency is limited to between 0.5% and 1% of the signal photons by

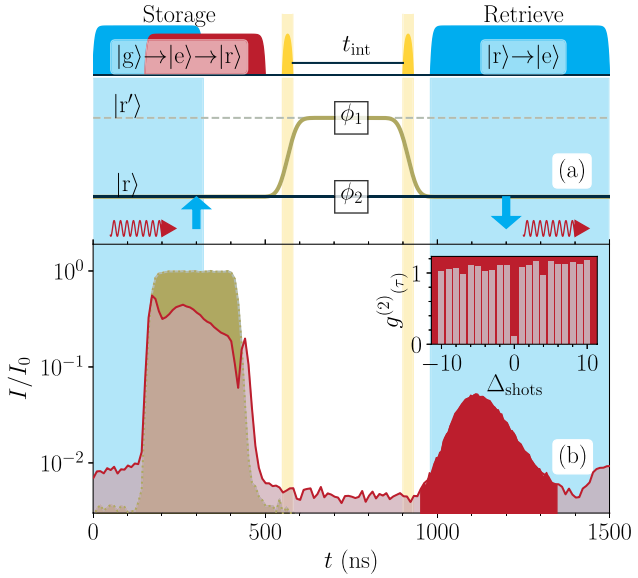

Fig. 1. Principle of the interferometer. (a) A photon (red arrow)—incident on a cold atom ensemble, and resonant with the $|g\rangle \rightarrow |e\rangle$ transition—is stored as an excitation in the Rydberg state $|r\rangle$, using a coupling field (blue arrow) resonant with the $|e\rangle \rightarrow |r\rangle$ transition. A microwave pulse (yellow) creates a superposition of two paths corresponding to internal quantum states, $|r\rangle$ and $|r'\rangle$. The superposition is maintained for a free evolution time, $t_{\rm int}$, and then recombined via a second microwave pulse. Finally, the population in $|r\rangle$ is read out by driving the transition $|r\rangle \rightarrow |e\rangle$ (blue). (b) Intensity measured during the complete sequence: storage ($t = 120 - 420$ ns), interferometer ($t = 560 - 920$ ns), and read-out $t = 950 - 1350$ ns. Inset: coincidence counts in a single shot and between shots indicating the single photon character of the stored light. For a Rydberg state $|r\rangle$ with principal quantum number $n = 90$.

blockade, the limited optical depth, and motional dephasing due to the finite temperature of the atomic ensembles.

After storage, the stored photon is "split" using a microwave field with linear polarization that couples the highly excited Rydberg state, $|r\rangle = |nS_{1/2}\rangle$, to another Rydberg state $|r'\rangle = |nP_{3/2}\rangle$, shown in yellow in Fig. 1(a). The microwave field amplitude is uniform over the dimensions of the stored photon. The microwave pulse, lasting 25 ns, is calibrated as a $\pi/2$ pulse to realize the superposition state $\frac{1}{\sqrt{2}}(|r\rangle + |r'\rangle)$. After a period of free evolution, $t_{\rm int}$, the microwave source drives another $\pi/2$ pulse to recombine the two paths. Finally, the population in $|r\rangle$ is measured by coupling this state back to $|e\rangle$ using the control field (shown in blue in Fig. 1). Each experimental run is performed thousands of times. A complete run consists of laser cooling and trapping for 120 ms followed by 20,000 individual interferometer measurements performed on the same ensemble in 90 ms. This gives an effective repetition rate of 95 kHz. All the cooling and trapping lasers are turned off during the interferometer measurements. The transmission of the probe beam is measured throughout using a single-photon counter [Fig. 1(b)]. More details on the experimental apparatus and the relevant atomic levels can be found in previous work [16–18].

We employ highly excited Rydberg states with principal quantum numbers in the range $n = 60 - 90$. The Rydberg blockade mechanism [12,19,20] limits the interferometer to only one photon at a time. To demonstrate this, we perform a Hanbury Brown Twiss (HBT) measurement on the light retrieved from the ensemble. The retrieved light is split by a 50:50 beam splitter and sent to two detectors. The normalized coincidence counts for a single retrieval is strongly suppressed [Fig. 1(b) (inset)]. For a Rydberg state $|r\rangle$ with principal quantum number $n = 90$, the probability to observe two photons in the same experimental shot, characterized by the normalized second-order intensity correlation, is $g^{(2)}(0) = 0.10 \pm 0.02$. The correlation function between successive shots $g^{(2)}(\tau)$ is unity, as expected.

The output of the interferometer has the form [1]

$$\mathcal{I} = \mathcal{I}_0(1 - \cos\phi), \tag{1}$$

where $\mathcal{I}_0$ is the maximum output of the interferometer, $\phi = \Delta_\mu t_{\rm int}$, and $\Delta_\mu = [\omega_\mu - (E_{|r'\rangle} - E_{|r\rangle})/\hbar]$ is the detuning of the microwave field. Consequently, to measure the interference fringes, we can either vary the microwave field frequency, ω_μ, or the superposition time, $t_{\rm int}$. Note that the phase ϕ and hence the intensity output are also sensitive to any perturbation in the energy levels, $E_{|r\rangle}$ and $E_{|r'\rangle}$. The interference fringes as a function of both the microwave field detuning, Δ_μ, and the superposition time, $t_{\rm int}$, are shown in Fig. 2. In Fig. 2(a), we show the fringes for $t_{\rm int} = 250$ ns. In the experiment, the visibility of the interference fringes is reduced by technical factors including the imperfect removal of population from the Rydberg manifold after each shot of the experiment, and imperfect polarization of the microwave fields. Future work will focus on improving these technical issues. In Fig. 2(b), we focus on the interference fringes in the range $\Delta_\mu/(2\pi) = -10$ to 10 MHz, and show the effect of varying the superposition time, $t_{\rm int}$. The data are overlaid with theoretical retrieval maxima in yellow. The color in the contour plot refers to $\mathcal{I}/\mathcal{I}_0$ for all figures. As expected, as we increase $t_{\rm int}$, the interferometer becomes more sensitive to changes in the relative phase. In the current experiment, $t_{\rm int}$ is limited to of order 1000 ns by motional dephasing [18], which scrambles the information about the stored photon.

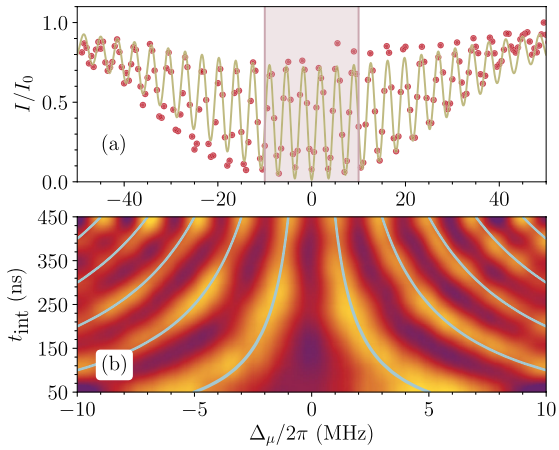

Fig. 2. Operation of the interferometer. (a) Output fringes of the single-photon interferometer by varying the detuning of the microwave field Δ_μ. The data (red dots) are obtained for a superposition time $t_{\rm int} = 250$ ns and fitted by solving the optical Bloch equations for the complete time sequence. Apart from an overall envelope, the fit has the form of Eq. (1). (b) Measured interferometric fringes as a function of both Δ_μ and the superposition time $t_{\rm int}$, for $t_{\rm int} \leq 450$ ns. For these data, we use $|r\rangle = |60S_{1/2}\rangle \rightarrow |r'\rangle = |59P_{3/2}\rangle$ transition, with resonant frequency 18.5 GHz. The lines show the theoretically predicted retrieval maxima.

Next, we demonstrate the sensitivity of the interferometer fringes to external fields. First, we apply a DC electric field. This has the effect of shifting the energy levels due to the DC Stark effect, i.e.,

$$\Delta E_{|r\rangle} = -\frac{1}{2}\alpha_{|r\rangle}\mathcal{E}^2, \tag{2}$$

where $\alpha_{|r\rangle}$ is the polarizability of the state $|r\rangle$, and $\mathcal{E}$ is the applied electric field. The external field is applied during the superposition time between the two microwave $\pi/2$ pulses [Fig. 3 (top)]. Figure 3(a) shows the interference fringes at zero field and a DC field of 6.3 V/m. At this field value, the phase shift is π. Note that the fringe contrast is conserved, as the DC field induces only a global phase shift, without perturbing the spatial mode of the photon. Figure 3(b) shows the fringe shift from 0 to 12 V/m, with the phase shift indicated on the right-hand axis. As expected, we observe a quadratic shift of the Ramsey fringes matching the relative DC Stark shift of states $|r\rangle$ and $|r'\rangle$.

Second, we investigate the sensitivity of our single-photon stored-light interferometer to an external AC electric field. In the case of AC fields, the polarizabilities, $\alpha_{|r\rangle}$ and $\alpha_{|r'\rangle}$, exhibit resonances at particular radio, microwave, and terahertz frequencies that match electric dipole allowed transitions between atomic Rydberg states, and these resonances have emerged as a promising platform for sensitive measurements of rf [22] and terahertz [23] fields. The sensitivity of the interferometer to a near-resonant external microwave field is predicted by the AC Stark shift of individual Rydberg states. The energy shift of a state $|i\rangle$ can be represented by

$$\Delta E_i = -\frac{\mathcal{E}^2}{4\hbar}\sum_{i\neq f}|\langle i|\mathbf{d}|f\rangle|^2\left(\frac{1}{\omega_{\mu 2}-\omega_{if}}+\frac{1}{\omega_{\mu 2}+\omega_{if}}\right), \tag{3}$$

where $\langle i|\mathbf{d}|f\rangle$ is the electric dipole moment for a transition between states $|i\rangle$ and $|f\rangle$, $\omega_{\mu 2}$ is the frequency of the external field, and ω_{if} is the resonant transition frequency between i and f. In the experiment, we use an interferometer based on the states $|r\rangle = 60S_{1/2}$ and $|r'\rangle = 59P_{3/2}$. The external microwave field is chosen to couple $|i\rangle = |r'\rangle = 59P_{3/2}$ to another Rydberg state $|f\rangle = |r''\rangle = 59S_{1/2}$. The resonant frequency for this case is 18.2 GHz, and the transition has a dipole moment, $\langle i|\mathbf{d}|f\rangle = 4107$ Debye [21]. The pulse sequence is shown in Fig. 4 (top). The additional microwave field (green) is applied during the interferometer superposition time between the two $\pi/2$ pulses (yellow). Figure 4(a) shows measurements of the single-photon Ramsey fringes as a function of both the detuning of the additional microwave field, $\Delta_{\mu 2} = \omega_{\mu 2} - \omega_{if}$, and the superposition time, $t_{\rm int}$. Figure 4(b) shows how the shift of the interference fringes follows a dispersive-like law, as expected. A fit to Eq. (3)—the dotted line in the figure—is in good agreement with the data.

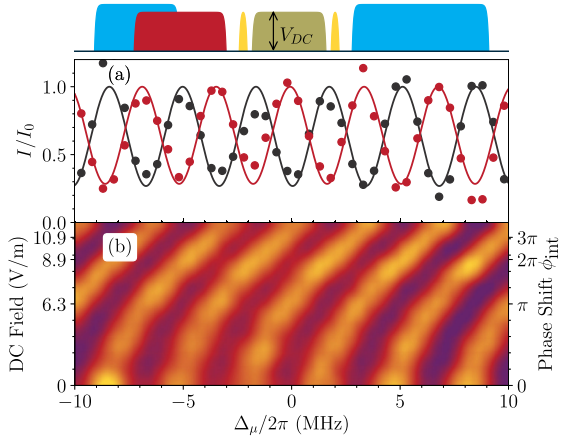

Fig. 3. Sensitivity of the single-photon interferometer to a DC electric field. Top: timing sequence is the same as in Fig. 1, i.e., photon storage, interferometer (yellow pulses), and retrieval, but with the addition of a DC electric field during the superposition time of the interferometer (green). (a) Measured interference fringes at a DC field of 0 V (black dots) and 6.3 V/m (red dots). The data are normalized to the zero-field interference fringe maxima. The solid line is a fit. (b) Colormap showing the electric-field-dependent phase shift of the interferometer fringes. The value of DC fields is calibrated using the known polarizabilities of the Rydberg states [21].

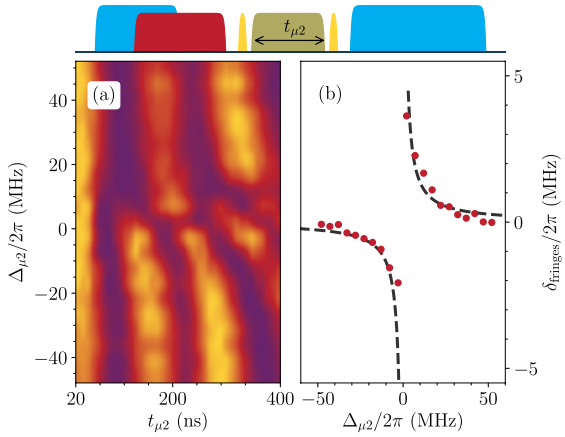

Fig. 4. Single-photon sensing of an external microwave field. Top: timing sequence as previously except now with an additional microwave field applied for a time $t_{\mu 2}$ during the interferometer superposition time. (a) Colormap showing measurements of the single-photon interference fringes as a function of both the detuning of the external field, $\Delta_{\mu 2}$, and the interferometer superposition time, $t_{\rm int}$ with $\Delta_\mu/(2\pi) = 8$ MHz. The external microwave field couples one path of the interferometer to another Rydberg state. (b) Frequency shift of the Ramsey fringes, $\delta_{\rm fringes}$, follows a dispersive-like law, as expected with detuning of $\Delta_{\mu 2}$. The dotted line shows a fit to Eq. (3).

An interesting feature of the stored-light interferometer is that it provides two ways of measuring an external rf field, first via a fringe shift as shown in Fig. 4, and second via the loss of visibility. Figure 5 shows rf sensing data in the vicinity of a resonance. Figure 5(a) shows the Ramsey fringes as a function of the detuning of the microwave field, Δ_μ, while varying detuning of the external rf field, $\Delta_{\mu 2} = \omega_{\mu 2} - \omega_{if}$. In contrast, to the DC field case, Fig. 3, now we observe a change in the fringes visibility in the vicinity of the microwave resonance. When the external field is close to a resonance with another Rydberg state, we see a dramatic loss of fringes contrast. This is plotted in Fig. 5(b). The loss occurs because there is a probability that a part of the photon energy is coupled into the microwave field similar to the classic decoherence experiment of Brune *et al.* [24]. The data are fitted with a lineshape that is consistent with Fourier transform of the microwave pulse duration of 200 ns. Compared to Fig. 4, this plot illustrates how the loss of coherence is more frequency selective than the phase shift, and could be used for high-resolution measurements of Rydberg transition frequencies, which are important in the determination of quantum defects [25].

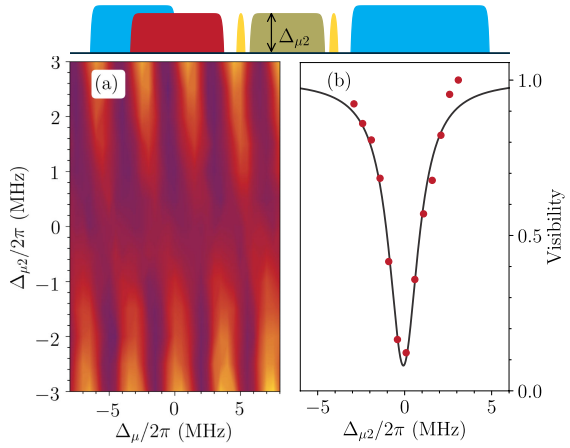

Fig. 5. Effect of an external rf field on the visibility of the single-photon interference fringes. Top: timing sequence same as Fig. 4 except that the duration of the external field is now fixed at $t_{\mu 2} = 200$ ns. (a) Colormap showing the single-photon interference fringes as a function, Δ_{μ}, and the detuning of the external field, $\Delta_{\mu 2}$, with $t_{\mathrm{int}} = 250$ ns. On this scale, $\Delta_{\mu 2} = -3$ to 3 MHz, the AC Stark shift seen in Fig. 4 is scarcely visible, whereas the loss of coherence is pronounced. (b) Plot of the fringe visibility in the vicinity of resonance with the external field. The data are fitted with a lineshape consistent with Fourier limited linewidth for a 200 ns rf pulse.

Applications of the single-photon interferometer will be explored in further work. For sensing applications, the current experiment is limited by shot noise (in contrast to classical measurements [11], quantum measurement is limited to only one photon per shot) and photon storage time. The latter could be greatly increased by eliminating motional dephasing of the spin wave, by using either a Doppler-free configuration [26] or an optical lattice to localize the atoms [27]. Ultimately, the fundamental limit is the lifetime of the Rydberg states, which for circular states can be > 1000 s [28]. Using these techniques, a stored-light interferometer could rival state-of-the-art electrometers [9,11,22].

In summary, we have realized a single-photon stored-light Ramsey-type interferometer via storing optical photons as Rydberg polaritons. The character of the Ramsey-like interference fringes has been demonstrated. We show that the interferometer, localized to a length scale of just a few micrometers, can be used to measure external fields. In these examples, information about the field is mapped onto the quantum state of the stored photon. This can lead to changes in both the fringe position and visibility. Our method paves the way towards advanced quantum probing of external fields. The advantage of our technique compared to beam experiments is that the interferometer is highly localized on the micrometer length scale, providing a "localized" probe of the external field. Potential applications include precision measurement of Rydberg transition frequencies, and localized sensing of fields, which perturbs either of the Rydberg states involved. The interferometer can be made sensitive to single optical photons by mapping them into Rydberg polaritons [29], and could be used as the basis to realize a photonic phase gate [30].

Funding. Engineering and Physical Sciences Research Council (EP/M014398/1, EP/R002061/1, EP/S015973/1).

Acknowledgment. The figure data are available on the Durham University Collections repository (doi:10.15128/r2r207tp335).

Disclosures. The authors declare no conflicts of interest.

REFERENCES

1. C. S. Adams and I. G. Hughes, *Optics F2f: From Fourier to Fresnel* (Oxford University, 2018).
2. R. Abbott, F. Acernese, K. Ackley, C. Adams, T. Adams, P. Addesso, and R. X. Adhikari, Phys. Rev. Lett. **116**, 061102 (2016).
3. C. S. Adams, M. Sigel, and J. Mlynek, Phys. Rep. **240**, 143 (1994).
4. N. F. Ramsey, Phys. Rev. **78**, 695 (1950).
5. N. F. Ramsey, Rev. Mod. Phys. **62**, 541 (1990).
6. Z. Shi, R. W. Boyd, R. M. Camacho, P. K. Vudyasetu, and J. C. Howell, Phys. Rev. Lett. **99**, 240801 (2007).
7. B. Chen, C. Qiu, S. Chen, J. Guo, L. Q. Chen, Z. Y. Ou, and W. Zhang, Phys. Rev. Lett. **115**, 043602 (2015).
8. C. Qiu, S. Chen, L. Q. Chen, B. Chen, J. Guo, Z. Y. Ou, and W. Zhang, Optica **3**, 775 (2016).
9. A. Facon, E.-K. Dietsche, D. Grosso, S. Haroche, J.-M. Raimond, M. Brune, and S. Gleyzes, Nature **535**, 262 (2016).
10. J. E. Palmer and S. D. Hogan, Phys. Rev. Lett. **122**, 250404 (2019).
11. A. Arias, G. Lochead, T. M. Wintermantel, S. Helmrich, and S. Whitlock, Phys. Rev. Lett. **122**, 053601 (2019).
12. M. D. Lukin, M. Fleischhauer, R. Cote, L. M. Duan, D. Jaksch, J. I. Cirac, and P. Zoller, Phys. Rev. Lett. **87**, 037901 (2001).
13. J. A. Sedlacek, A. Schwettmann, H. Kübler, R. Löw, T. Pfau, and J. P. Shaffer, Nat. Phys. **8**, 819 (2012).
14. H. Fan, S. Kumar, J. Sedlacek, H. Kübler, S. Karimkashi, and J. P. Shaffer, J. Phys. B **48**, 202001 (2015).
15. C. G. Wade, N. Šibalić, N. R. de Melo, J. M. Kondo, C. S. Adams, and K. J. Weatherill, Nat. Photonics **11**, 40 (2017).
16. C. Möhl, N. L. R. Spong, Y. Jiao, C. So, T. Ilieva, M. Weidemüller, and C. S. Adams, J. Phys. B **53**, 084005 (2020).
17. H. Busche, S. W. Ball, and P. Huillery, Eur. Phys. J. Spec. Top. **225**, 2839 (2016).
18. H. Busche, P. Huillery, S. W. Ball, T. Ilieva, M. P. Jones, and C. S. Adams, Nat. Phys. **13**, 655 (2017).
19. L. Li and A. Kuzmich, Nat. Commun. **7**, 13618 (2016).
20. D. P. Ornelas-Huerta, A. N. Craddock, E. A. Goldschmidt, A. J. Hachtel, Y. Wang, P. Bienias, A. V. Gorshkov, S. L. Rolston, and J. V. Porto, "On-demand indistinguishable single photons from an efficient and pure source based on a Rydberg ensemble," arXix:2003.02202 (2020).
21. N. Šibalić, J. Pritchard, C. Adams, and K. Weatherill, Comput. Phys. Commun. **220**, 319 (2017).
22. M. Jing, Y. Hu, J. Ma, H. Zhang, L. Zhang, L. Xiao, and S. Jia, Nat. Phys. **16**, 911 (2020).
23. L. A. Downes, A. R. MacKellar, D. J. Whiting, C. Bourgenot, C. S. Adams, and K. J. Weatherill, Phys. Rev. X **10**, 011027 (2020).
24. M. Brune, E. Hagley, J. Dreyer, X. Maître, A. Maali, C. Wunderlich, J. M. Raimond, and S. Haroche, Phys. Rev. Lett. **77**, 4887 (1996).
25. W. Li, I. Mourachko, M. W. Noel, and T. F. Gallagher, Phys. Rev. A **67**, 052502 (2003).
26. N. Šibalić, J. M. Kondo, C. S. Adams, and K. J. Weatherill, Phys. Rev. A **94**, 033840 (2016).
27. U. Schnorrberger, J. D. Thompson, S. Trotzky, R. Pugatch, N. Davidson, S. Kuhr, and I. Bloch, Phys. Rev. Lett. **103**, 033003 (2009).
28. T. L. Nguyen, J. M. Raimond, C. Sayrin, R. Cortiñas, T. Cantat-Moltrecht, F. Assemat, I. Dotsenko, S. Gleyzes, S. Haroche, G. Roux, T. Jolicoeur, and M. Brune, Phys. Rev. X **8**, 011032 (2018).
29. D. Paredes-Barato and C. S. Adams, Phys. Rev. Lett. **112**, 040501 (2014).
30. D. Tiarks, S. Schmidt-Eberle, T. Stolz, G. Rempe, and S. Dürr, Nat. Phys. **15**, 124 (2019).